

Dinucleon correlation of ${}^9\text{Li}$, ${}^{10}\text{Be}$, and ${}^{9,10}\text{C}$

Fumiharu Kobayashi and Yoshiko Kanada-En'yo

Department of Physics, Kyoto University, Kyoto 606-8502, Japan

(Dated: September 30, 2018)

We study the dinucleon (dineutron and diproton) correlation of the ground states of ${}^9\text{Li}$, ${}^{10}\text{Be}$, and ${}^{9,10}\text{C}$. We assume an $\alpha + t$ core for ${}^9\text{Li}$, an $\alpha + \alpha$ core for ${}^{10}\text{Be}$ and ${}^{10}\text{C}$, and an $\alpha + {}^3\text{He}$ core for ${}^9\text{C}$, and investigate the effect of core structure changes on the degree of dineutron formation and spatial expansion from the core. For ${}^9\text{Li}$, t cluster breaking in the core significantly enhances the dineutron component inside the nuclei. Moreover, its component markedly depends on the strength of the spin-orbit interaction since a dineutron is fragile and dissociates readily due to the spin-orbit interaction. Compared with ${}^9\text{Li}$, the dineutron of ${}^{10}\text{Be}$ dissociates largely due to the stronger spin-orbit attraction from the $\alpha + \alpha$ core than the $\alpha + t$ core. We also investigate diproton features in ${}^{9,10}\text{C}$, the mirror nuclei of ${}^9\text{Li}$ and ${}^{10}\text{Be}$, respectively, and compare them with the dineutron features of ${}^9\text{Li}$ and ${}^{10}\text{Be}$. No qualitative difference is observed between diprotons and dineutrons in the degree of formation at the surface, but a quantitative difference may exist in the degree of dinucleon-size change far from the core.

I. INTRODUCTION

Recently, neutron-rich nuclei have been investigated in detail and they have been found to play a major role in many exotic phenomena. Dineutron correlation is one of the most interesting topics in the physics of neutron-rich nuclei. A dineutron is a spatially compact spin-singlet pair of two neutrons. Although two neutrons are not bound in free space, it is theoretically suggested that dineutron correlation may be enhanced and a compact dineutron is formed in some situations such as in a low-density region of nuclear matter [1, 2] and in the neutron-halo and neutron-skin regions of finite neutron-rich nuclei [3–10]. Since a spin-singlet pair of two neutrons is unbound, a dineutron is fragile and its features, such as the degree of formation and size, can readily change depending on the circumstance. For example, in neutron matter, it was suggested that the strength of the spatial correlation between two neutrons depends markedly on the neutron density. The transition between the spatially weak pairing (BCS-like (Bardeen-Cooper-Schrieffer-like) pairing) and the spatially strong pairing (boson-like pairing) under a changing neutron density was discussed in relation to the BCS-BEC (Bose-Einstein condensate) crossover [2]. In finite nuclei, especially in a neutron-rich nucleus such as ${}^{11}\text{Li}$, dineutron correlation is markedly enhanced at the nuclear surface and the relative distance between two neutrons in a dineutron becomes typically 2 – 3 fm such that a dineutron may be regarded as a kind of cluster (boson) since the distance of separation is much smaller than the size of the total system. As is well known, finite nuclei show various structures of deformation, clusterization, neutron-halo or neutron-skin, etc. Such diverse structures may affect dineutron correlation. To clarify the universal properties of dineutron correlation in finite nuclei, we constructed a model of a dineutron condensate (DC) wave function [11], which describes the behavior of a dineutron around a core in detail. This model requires no assumptions about the core structure so that this model is useful to systematically investigate

dineutron features in typical neutron-rich nuclei. We applied this model to ${}^{10}\text{Be}$ (2α core+ $2n$) and investigated dineutron formation around the 2α core [11]. We found that a compact dineutron is formed just at the nuclear surface and it spreads somewhat far from the core keeping a compact size in the ${}^{10}\text{Be}$ ground state. We suggested that a dineutron would be formed in typical nuclei.

In this work, we investigate dineutron correlation in the ${}^9\text{Li}$ ground state (${}^7\text{Li}$ core+ $2n$) and clarify the effect of ${}^7\text{Li}$ core structure change on dineutron correlation. We mainly discuss dineutron features and, in particular, the degrees of formation and spatial expansion from the core. Free ${}^7\text{Li}$ is well described by the $\alpha + t$ cluster structure. However, the t cluster in the ${}^7\text{Li}$ core of ${}^9\text{Li}$ is deeply bound and more or less fragile, so it is expected that t cluster breaking would be an important aspect of the ${}^7\text{Li}$ core description. This is rather different from the $\alpha + \alpha$ core in ${}^{10}\text{Be}$ where α cluster breaking is minor. We describe the ${}^7\text{Li}$ core as the $\alpha + t$ structure and take into account t cluster breaking in addition to its spatial development as a change in the ${}^7\text{Li}$ core structure. We also investigate the effect of such core structure changes on dineutron features around the core by applying a DC wave function. We also compare the dineutron behavior of ${}^9\text{Li}$ and ${}^{10}\text{Be}$ to clarify the difference between dineutron features around the $\alpha + t$ and $\alpha + \alpha$ cores.

Furthermore, we investigate the spatial correlation between two protons in the spin-singlet channel of proton-rich nuclei, a phenomenon that is called diproton correlation. Since the Coulomb repulsive force acts between two protons, diproton correlation may vary qualitatively or quantitatively from dineutron correlation. Experimental and theoretical studies suggest that diproton correlation is just as likely as dineutron correlation in spite of the Coulomb interaction between two protons [12–19]. In this work, we also investigate the difference between dineutron and diproton features by comparing the diproton correlation of ${}^{9,10}\text{C}$ with the dineutron correlation of ${}^9\text{Li}$ and ${}^{10}\text{Be}$, since ${}^{9,10}\text{C}$ are the mirror nuclei of ${}^9\text{Li}$ and ${}^{10}\text{Be}$, respectively.

The content of this paper is as follows. In Sec. II, we describe the framework used in the present study. In Sec. III, we examine dineutron correlation results in the ground states of ${}^9\text{Li}$ and ${}^{10}\text{Be}$. We first evaluate the dineutron probability for ${}^9\text{Li}$ and consider the effect of core structure change on dineutron features. Next, we compare the dineutron features of ${}^9\text{Li}$ with those of ${}^{10}\text{Be}$ and demonstrate that their differences arise from the core structure. In Sec. IV, we discuss the diproton features of ${}^9\text{C}$ and ${}^{10}\text{C}$ and compare them with dineutron features in their mirror nuclei ${}^9\text{Li}$ and ${}^{10}\text{Be}$, respectively. Finally, we provide a summary of the present work in Sec. V.

II. FRAMEWORK

In this section, we first describe the framework used to investigate the dineutron correlation of ${}^9\text{Li}$. The framework used for both ${}^{10}\text{Be}$ and ${}^9,{}^{10}\text{C}$ is similar to that employed for ${}^9\text{Li}$, and only a brief explanation is subsequently added concerning these latter nuclei.

To investigate dineutron correlation in the ${}^9\text{Li}$ ground state, we superpose two kinds of wave functions: one to describe the main structure of the ground state and the other to efficiently describe the dineutron correlation about the ${}^7\text{Li}$ core. For the former, we use the ${}^6\text{He}+t$ cluster wave function as proposed in Ref. [20], which was previously used to describe the ${}^9\text{Li}$ system as ${}^6\text{He}(\alpha + 2n[(0p)^2])$ plus t clusters. By using such a wave function, the low-lying energy spectrum of ${}^9\text{Li}$ can be well reproduced. For the latter, we use a DC wave function having an $\alpha + t$ core. This DC wave function can describe the detailed features of a dineutron about the core, that is, the size change of the dineutron and the expansion of the dineutron distribution from the core [11, 21, 22]. By superposing these wave functions, we investigate the competition between dineutron formation (wherein two neutrons couple to a spin singlet with spatial correlation) and its dissociation at the surface due to spin-orbit interaction (wherein two neutrons are in the major shell independently) and the expansion of the dineutron distribution far from the core. The ${}^6\text{He}+t$ cluster wave function can describe spin-singlet pair formation and pair dissociation to the $(0p_{3/2})^2$ configuration of two neutrons just at the surface of the $\alpha + t$ core. Using the DC wave function, we consider the dineutron spatial expansion from the core and the dineutron-size change. We investigate the effect of the $\alpha + t$ core structure change on such dineutron features as the dineutron formation and dissociation near the surface and its expansion from the core. For this purpose, we take into account t cluster breaking and development in the $\alpha + t$ core of the DC wave function as well as that in the ${}^6\text{He}+t$ cluster wave function. For t cluster breaking, we introduce the method proposed by Itagaki *et al* to break a cluster to gain the spin-orbit energy [23].

In the following, we first describe the details of the ${}^6\text{He}+t$ cluster wave function and the ${}^9\text{Li}$ DC wave func-

tion without t cluster breaking. Subsequently, we explain t cluster breaking in the core.

A. The ${}^6\text{He}+t$ cluster wave function

First, we explain the simple ${}^6\text{He}+t$ cluster wave function proposed in Ref. [20] without t cluster breaking. For the ${}^6\text{He}+t$ cluster wave function, the ${}^9\text{Li}$ system consists of the ${}^6\text{He}$ cluster and the t cluster, with the cluster wave functions being described by the Bloch-Brink wave function [24]. The ${}^6\text{He}$ cluster is composed of a $(0s)^4$ α cluster and two valence neutrons in harmonic oscillator (H.O.) $(0p)^2$ configurations around the α . The ${}^6\text{He}+t$ cluster wave function, $\Phi_{{}^6\text{He}+t}$, is as follows.

$$\Phi_{{}^6\text{He}+t}(\kappa, d_t) = \mathcal{A} \left\{ \Phi_{{}^6\text{He}}(\kappa, \mathbf{R}_{{}^6\text{He}} = -d_t/3 \mathbf{e}_z) \times \Phi_t(\mathbf{R}_t = 2d_t/3 \mathbf{e}_z) \right\}, \quad (1)$$

where $\Phi_{{}^6\text{He},t}$ are the wave functions of the ${}^6\text{He}$ and t clusters. The t cluster is composed of a spin-up proton and spin-up and spin-down neutrons. Here, the t cluster is an ideal $(0s)^3$ t cluster, which we define as a t cluster. The spatial component of the single-particle wave function, ϕ , is described with the Gaussian wave packet as

$$\phi(\mathbf{r}; \nu, \mathbf{R}) \propto \exp[-\nu(\mathbf{r} - \mathbf{R})^2]. \quad (2)$$

In the ${}^6\text{He}$ cluster, two valence neutrons are in the $0p$ configurations described by a shifted Gaussian from the α , and κ assigns the $0p$ configuration of two valence neutrons around the α . $\mathbf{R}_{{}^6\text{He},t}$ are the center of mass of the Gaussian center parameters in the ${}^6\text{He}$ and t clusters, and the ${}^6\text{He}$ and t clusters are separated by a distance d_t in the z -direction. The Gaussian width parameter, ν , is chosen as $\nu = 0.235 \text{ fm}^{-2}$ for all nucleons. A schematic representation of the ${}^6\text{He}+t$ cluster wave function is shown

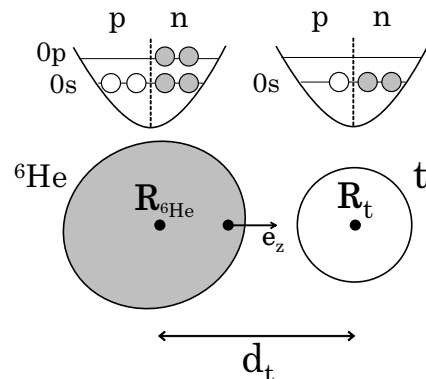


FIG. 1: A schematic representation of the ${}^6\text{He}+t$ cluster wave function. ${}^6\text{He}$ is described with $\pi[(0s)^2]\nu[(0s)^2(0p)^2]$ configurations around $\mathbf{R}_{{}^6\text{He}}$. The t cluster contains a spin-up proton and spin-up and spin-down neutrons in the $0s$ orbit around \mathbf{R}_t .

in Fig. 1. By using the ${}^6\text{He}+t$ cluster wave function, we describe the main structure of the ${}^9\text{Li}$ ground state. This wave function can describe two valence neutrons in H.O. $(0p)^2$ configurations, and, therefore, the mixing of configuration κ describes the competition between dineutron formation (wherein two neutrons couple to the spin singlet in the $0p$ shell) and dineutron dissociation (wherein two neutrons occupy the $(0p_{3/2})^2$ to gain the spin-orbit interaction) just at the surface.

B. The ${}^9\text{Li}$ DC wave function

In addition to the ${}^6\text{He}+t$ cluster wave functions, we superpose the DC wave functions [11] for ${}^9\text{Li}$ to describe dineutron correlation around the $\alpha+t$ core. The present DC wave function describes the system composed of the $\alpha+t$ core and one dineutron of a pair of spin-up and spin-down neutrons. For the ${}^9\text{Li}$ DC wave function, the dineutron is distributed around the core spherically changing its size and spatial expansion from the core as follows.

$$\Phi_{\text{DC}}(d_t, \beta, b_n) = \mathcal{A}\{\Phi_{\alpha+t}(d_t) \times \Phi_{2n_{\text{DC}}}(\beta, b_n)\} \quad (3)$$

$$\Phi_{2n_{\text{DC}}}(\beta, b_n) = \mathcal{A}\{\psi_r(b_n)\psi_G(\beta) \chi_{\uparrow}(n1)\chi_{\downarrow}(n2)\}, \quad (4)$$

$$\psi_r(\mathbf{r}; b_n) \propto \exp\left[-\frac{r^2}{4b_n^2}\right], \quad (5)$$

$$\psi_G(\mathbf{r}_G; \beta) \propto \exp\left[-\frac{r_G^2}{\beta^2}\right]. \quad (6)$$

$\Phi_{\alpha+t, 2n_{\text{DC}}}$ are the wave functions of the $\alpha+t$ core and the dineutron. The dineutron wave function, $\Phi_{2n_{\text{DC}}}$, is composed of the relative and center-of-mass wave functions of the two neutrons forming the dineutron, ψ_r and ψ_G , where $\chi_{\uparrow/\downarrow}$ are the spin-up and spin-down wave functions. The coordinate $\mathbf{r} = \mathbf{r}_{n1} - \mathbf{r}_{n2}$ is a distance relative to the two neutrons in the dineutron, given by the coordinates $\mathbf{r}_{n1, n2}$, while $\mathbf{r}_G = (\mathbf{r}_{n1} + \mathbf{r}_{n2})/2$ is their center-of-mass relative to the origin. For the DC wave function, a spin-singlet dineutron is composed of two neutrons in

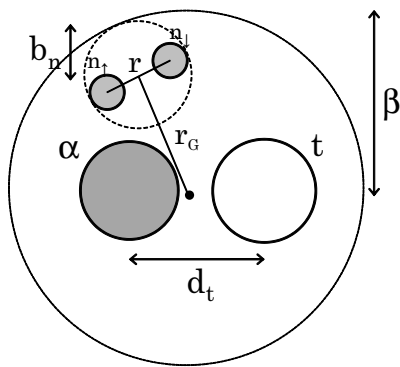


FIG. 2: A schematic representation of the ${}^9\text{Li}$ DC wave function. b_n stands for the dineutron size and β stands for the dineutron expansion from the core. The core is described with the α and t clusters separated by d_t .

the relative s wave and it is distributed about the origin in the S wave. In the relative wave function, ψ_r , two neutrons have the same size parameter, b_n ($\nu = (2b_n^2)^{-1}$ in Eq. (2)), characterizing the relative distance between two neutrons, that is, the dineutron size. In the center-of-mass wave function, ψ_G , the spatial expansion of the dineutron is characterized by the parameter β . (By definition, $\beta > b_n$ as shown in Ref. [11].) A schematic representation of the ${}^9\text{Li}$ DC wave function is shown in Fig. 2.

In the DC wave function, we change these characteristic parameters (β, b_n) to various values to evaluate detailed dineutron behavior. When b_n is small, the distance between two neutrons is small and a compact dineutron is formed. On the other hand, when $b_n \approx \beta$, the DC wave function corresponds to the state where each valence neutron is in the s wave with the width $b_n \approx \beta$ around the origin, as shown in Ref. [11]. Two neutrons in the s wave no longer exhibit spatial correlation and the dineutron disperses. Therefore, the DC wave function can describe dineutron formation and dispersion by changing the size parameter b_n . The parameter β corresponds to the degree of dineutron expansion from the core. When β is small, the dineutron is distributed near the core, and, when β is large, the dineutron distribution is widely expanded from the core. In such a way, the parameters b_n and β characterize the dineutron features of size and distribution about the core. We superpose DC wave functions consisting of various sets of (β, b_n) to describe a system containing a dineutron having various sizes and spatial distributions about the core.

For the ${}^9\text{Li}$ DC wave function, the core is described by the $\alpha+t$ cluster wave function, $\Phi_{\alpha+t}$. The α and t clusters, separated by a distance d_t , are described with the ideal $(0s)^4$ and $(0s)^3$ configurations, respectively. The center of mass of the ${}^7\text{Li}$ core is located at the origin and we omit the core recoil with respect to dineutron motion in the DC wave function. The Gaussian width of nucleons in the $\alpha+t$ core is fixed to $\nu = 0.235 \text{ fm}^{-2}$.

C. Development and breaking of the t cluster

Here, we examine the $\alpha+t$ core structure change. In the ${}^6\text{He}+t$ cluster wave function and the ${}^9\text{Li}$ DC wave function explained above, the system contains the $\alpha+t$ core, and the $\alpha-t$ relative distance is characterized by d_t . To describe the ${}^9\text{Li}$ ground state, we superpose wave functions with various d_t values and take into account the spatial development of the t cluster in the $\alpha+t$ core.

We also consider t cluster breaking in the $\alpha+t$ core as the core structure change. While the $\alpha+t$ threshold energy in free ${}^7\text{Li}$ is 2.47 MeV, the ${}^6\text{He}+t$ threshold energy in ${}^9\text{Li}$ is 7.59 MeV. The t cluster is deeply bound in ${}^9\text{Li}$ and t cluster breaking is expected at the surface, especially because spin-orbit interaction to occupy the $0p_{3/2}$ orbits is important in ${}^9\text{Li}$. Thus, we introduce t cluster breaking in the core in addition to t cluster development, and we also discuss the effect of core cluster breaking

on dineutron features. Here, we examine the method by which t cluster breaking is accounted for.

In a Gaussian-type, single-particle wave function [Eq. (2)], the real and imaginary parts of the center parameter, \mathbf{R} , correspond to the mean position and momentum of the particle, respectively.

$$\langle \mathbf{r} \rangle = \text{Re}[\mathbf{R}], \quad (7)$$

$$\langle \mathbf{p} \rangle = 2\hbar\nu\text{Im}[\mathbf{R}]. \quad (8)$$

For the ${}^6\text{He}+t$ cluster and ${}^9\text{Li}$ DC wave functions described in the previous sections, the t cluster is described using the ideal $(0s)^3$ configuration and the nucleons located there have the same real center parameter. We extend this framework to address breaking of the ideal $(0s)^3$ t cluster by giving the imaginary part (i.e., the momentum) to each center parameter of the nucleons in the cluster, as done in Ref. [23]. The momentum direction is fixed to be orthogonal to the nucleon spin direction and it is opposite for spin-up and spin-down nucleons to obtain spin-orbit attraction. The t cluster is located in the direction of \mathbf{e}_z from the other cluster, and the spins of one proton and neutron in the t cluster are oriented to the $-\mathbf{e}_x$ direction while the spins of the other neutron is oriented in the \mathbf{e}_x direction. Then, we choose the momentum direction to be \mathbf{e}_y , and we define the center parameters of the spin-up and spin-down nucleons in the t cluster as $\mathbf{R}_{\uparrow/\downarrow} = d_t\mathbf{e}_z \pm i\lambda_t\mathbf{e}_y$ (d_t, λ_t ; real) in the rest frame of the α cluster. The center of mass of the ${}^6\text{He}+t$ or $\alpha+t$ cluster wave function is fixed to the origin. λ_t characterizes the magnitude of the momentum of the nucleon in the t cluster, or, in other words, the degree of t cluster breaking. When $\lambda_t = 0$, the t cluster has the ideal $(0s)^3$ configuration, while, when λ_t is finite, the t cluster is broken. In the case of $\lambda_t = d_t$ in the $d_t \rightarrow 0$ limit, one proton and two neutrons in the t cluster occupy the H.O. $0p_{3/2}$ orbits around the α cluster. In this way, t cluster breaking can be taken into account by changing the λ_t value. It should be noted that the occupation probability of the single-particle orbits (mainly the ratio between the $0p_{3/2}$ and $0p_{1/2}$ orbits) in the core is changed by introducing t cluster breaking. We apply this method to the t cluster in the ${}^6\text{He}+t$ cluster wave function and the ${}^9\text{Li}$ DC wave function, and we consider t cluster breaking as the change in core structure as well as t cluster development.

D. Projection and superposition of wave functions

We describe ${}^9\text{Li}$ by superposing the ${}^6\text{He}+t$ cluster wave functions and the ${}^9\text{Li}$ DC wave functions. The t cluster in each wave function can be broken using the method

shown in Sec. II C.

$$\Psi_M^{J\pi} = \sum_K \left(\sum_i c_{Ki} \mathcal{P}_{MK}^{J\pi} \Phi_{{}^6\text{He}+t}(\kappa, \lambda_t, d_t) + \sum_j c_{Kj} \mathcal{P}_{MK}^{J\pi} \Phi_{\text{DC}}(\lambda_t, d_t, \beta, b_n) \right). \quad (9)$$

The parameter λ_t , which characterizes the degree of t cluster breaking, is added to each wave function [Eqs. (1) and (3)]. i and j are the abbreviations of $i = \{\kappa, \lambda_t, d_t\}$ and $j = \{\lambda_t, d_t, \beta, b_n\}$. $\mathcal{P}_{MK}^{J\pi}$ is the projection operator to the eigenstate having the total spin-parity of J^π . In the present work, we consider only the ground state of ${}^9\text{Li}$ with $J^\pi = 3/2^-$. The coefficients c_{Ki} and c_{Kj} in Eq. (9) are determined by diagonalizing the Hamiltonian in Sec. III A.

By superposing the ${}^6\text{He}+t$ cluster wave function, we describe the main structure of the ${}^9\text{Li}$ ground state. This wave function describes the competition between the configurations of the two valence neutrons near the $\alpha+t$ core, that is, mainly, the spin-singlet configuration (dineutron formation) in the p shell and the $(0p_{3/2})^2$ configuration (dineutron dissociation due to the spin-orbit interaction). By superposing the ${}^9\text{Li}$ DC wave function, we describe a dineutron whose size and spatial expansion from the core can change. We discuss how t cluster breaking and development affect the dineutron component near and far from the core. Although we do not take into account that the dineutron component far from the $\alpha+t$ core is dissociated due to the spin-orbit interaction, the $(0p_{3/2})^2$ configuration just at the surface is expected to be the dominant component of the dissociated dineutron for ${}^9\text{Li}$.

We examine the adopted parameters in the superposition of Eq. (9). To clarify the effects of t cluster breaking on dineutron correlation, we perform the calculations with and without t cluster breaking. In the calculation with t cluster breaking, we choose $\lambda_t = 0.0, 0.4$, and 0.8 fm for both the ${}^6\text{He}+t$ wave functions and the ${}^9\text{Li}$ DC wave functions. In the calculation without t cluster breaking, we fix λ_t at 0.0 fm. In both calculations, the relative distance between the ${}^6\text{He}$ or α cluster and the t cluster is chosen as $d_t = 1, 2, \dots, 5$ fm for each value of λ_t to consider t cluster development. By comparing the results obtained from the calculations with and without t cluster breaking, we can evaluate the effects of t cluster breaking.

In addition to the parameters (λ_t, d_t) characterizing the core structure, each wave function has parameters characterizing the behavior of the two valence neutrons around the core. For the ${}^6\text{He}+t$ cluster wave function, the parameter κ labels the $(0p)^2$ configurations of the two valence neutrons around the α cluster. We perform configuration mixing by superposing the wave functions with κ as done in Ref. [20]. The ${}^9\text{Li}$ DC wave function has two parameters, b_n and β , characterizing the dineutron size and the spatial expansion of the dineutron distribution from the core. We superpose $\beta = 2, 3, \dots, 6$ fm and four

b_n values are determined for each β as

$$b_n = 1.5 \times \left(\frac{\beta - 0.2}{1.5} \right)^{(i-1)/(4-1)} \quad (i = 1, \dots, 4). \quad (10)$$

These parameter choices are sufficient to describe the compact dineutron about the $\alpha + t$ core in the rather compact ground state of ${}^9\text{Li}$.

Next, we examine the framework used to describe the other nuclei. In the case of ${}^{10}\text{Be}$, we consider dineutron features around the $\alpha + \alpha$ core by superposing the ${}^6\text{He} + \alpha$ cluster wave functions and the ${}^{10}\text{Be}$ DC wave functions. Also, for ${}^{10}\text{Be}$, we take into account cluster breaking of one of the α clusters. The adopted parameters in the superposed wave functions are the same as those described for the ${}^9\text{Li}$ case. We project the superposed wave functions to $J^\pi = 0^+$ for the ${}^{10}\text{Be}$ ground state. As for the mirror nuclei, ${}^9\text{C}$ and ${}^{10}\text{C}$, we merely exchange protons and neutrons in the framework adopted for ${}^9\text{Li}$ and ${}^{10}\text{Be}$, respectively.

E. Measurement of the dinucleon component

The aim of this work is to investigate the dinucleon components of ${}^9\text{Li}$, ${}^{10}\text{Be}$, and ${}^{9,10}\text{C}$, and to discuss their possible dinucleon features. We define two measurements of the dineutron component around the core for each purpose. We mainly describe their definitions for the case of ${}^9\text{Li}$ and add definitions as necessary for the other nuclei afterwards.

The first measurement is the overlap with a DC wave function. The purpose of this overlap is to evaluate the dineutron size and expansion around a certain core in the state

$$\mathcal{N}_{\text{DC}}(\beta, b_n) = |\langle \mathcal{P}_{MK}^{3/2^-} \Phi_{\text{DC}}(\beta, b_n) | \Psi_M^{3/2_1^-} \rangle|^2, \quad (11)$$

where $\Psi_M^{3/2_1^-}$ is the ground state wave function of ${}^9\text{Li}$ calculated as Eq. (9). Φ_{DC} is the test DC wave function whose core is $\alpha + t$ and has two characteristic parameters: the dineutron size, b_n , and its expansion from the core, β . We prepare a certain $\alpha + t$ core wave function for the test DC wave function. In the present work, the $\alpha + t$ core structure is characterized by two parameters: the degree of t breaking, λ_t , and the α - t distance, d_t . We fix the parameters (λ_t, d_t) to optimum values, change the parameters (β, b_n) to various values, and observe how much the dineutron probability depends on the dineutron size and expansion about the specified core. We use this measurement in Sec. IV to investigate the degree of dinucleon-size change for ${}^9\text{Li}$ and ${}^9\text{C}$.

The second measurement determines the compact dineutron probability at a certain distance around the $\alpha + t$ core with consideration for the degree of core cluster development. For the test wave function, we fix the dineutron size to a certain value and specify the distance between the compact dineutron and the $\alpha + t$ core as

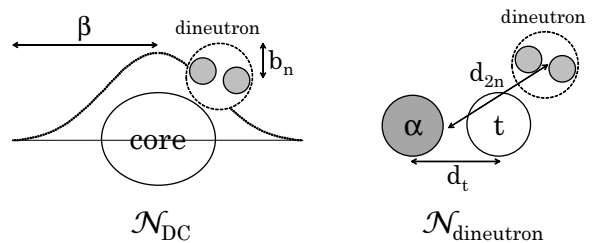


FIG. 3: Schematic representation of the two types of wave functions used for the \mathcal{N}_{DC} (left) and $\mathcal{N}_{\text{dineutron}}$ (right) measurements. In \mathcal{N}_{DC} , the key parameters are b_n (the dineutron size) and β (the dineutron expansion from the core). In $\mathcal{N}_{\text{dineutron}}$, the key parameters are d_{2n} (the core-dineutron distance) and d_t (the α - t distance).

well as the distance between the α and t clusters in the core. The overlap for the second measurement is written as follows.

$$\mathcal{N}_{\text{dineutron}}(d_{2n}, d_t) = |\langle \Phi_{\text{dineutron}}(d_{2n}, d_t) | \Psi_M^{3/2_1^-} \rangle|^2, \quad (12)$$

where $\Phi_{\text{dineutron}}$ is the wave function containing the compact dineutron of a fixed size ($\nu = 0.22 \text{ fm}^{-2}$) spherically distributed around the $\alpha + t$ core at a certain distance. The distance between the dineutron and the $\alpha + t$ core is specified by d_{2n} , and that between the α and t clusters in the core is specified by d_t . For the overlap of ${}^9\text{Li}$ with t cluster breaking, we take into account t cluster breaking in the $\alpha + t$ core of the test wave function as well. The details of these overlaps, $\mathcal{N}_{\text{dineutron}}$, are described in the appendix. In the present work, we use this measurement to evaluate core structure changes on the dineutron in ${}^9\text{Li}$, and to compare dinucleon features in ${}^9\text{Li}$, ${}^{10}\text{Be}$, and ${}^{9,10}\text{C}$.

Schematic representations of the two types of test wave functions of each overlap are shown in Fig. 3. The overlap involving the DC wave function, \mathcal{N}_{DC} [Eq. (11)], is a measurement of the dineutron size, b_n , and its expansion, β , from the core. It is noted here that the expansion, β , is not a distance but a degree of spatial expansion from the core. On the other hand, the second measurement, $\mathcal{N}_{\text{dineutron}}$ [Eq. (12)], evaluates the core-dineutron distance, d_{2n} , and the α - t distance in the core, d_t , for a dineutron size fixed at a certain value.

The compact dineutron probability, $\mathcal{N}_{\text{dineutron}}$, of the ${}^{10}\text{Be}$ ground state is defined similarly to Eq. (12). For ${}^{10}\text{Be}$, the core is $\alpha + \alpha$. Measurement of the diproton probability for ${}^{9,10}\text{C}$ is conducted the same as that for ${}^9\text{Li}$ and ${}^{10}\text{Be}$ except that protons and neutrons are exchanged.

III. DINEUTRON CORRELATION IN ${}^9\text{Li}$ AND ${}^{10}\text{Be}$

In this section, we discuss the degree of dineutron formation in the inner and surface regions and the de-

gree of dineutron expansion in the outer region in the ground states of ${}^9\text{Li}$ and ${}^{10}\text{Be}$. Comparing the results with and without t cluster breaking, we clarify the effect of core structure changes on the dineutron features of ${}^9\text{Li}$. We also discuss the interaction dependence of the dineutron probability. Additionally, we compare the dineutron probability of ${}^9\text{Li}$ with that of ${}^{10}\text{Be}$ and discuss the differences in the dineutron features arising from core structure differences.

A. Hamiltonian

In the present work, we use the Hamiltonian

$$H = T - T_G + V_{\text{cent}} + V_{\text{LS}} + V_{\text{Coul}}, \quad (13)$$

where T and T_G are the total and center-of-mass kinetic energies. Because all of the Gaussian widths of the DC wave function are not equal, the center-of-mass motion cannot be removed exactly. We therefore treat the center-of-mass motion approximately by extracting the expectation value of the center-of-mass kinetic energy, T_G , from the total Hamiltonian. V_{Coul} is the Coulomb force that is approximated by the summation of seven Gaussian functions. V_{cent} and V_{LS} are the effective central and spin-orbit interactions for which we use the Volkov No.2 force [25] and the spin-orbit part of the G3RS force [26], respectively. In this work, we choose the Majorana (m) parameter $m = 0.58$, the Bartlett (b) and Heisenberg (h) parameters $b = h = 0.0$ in V_{cent} , and the strength of $v_{\text{LS}} = 1600$ MeV in V_{LS} . This v_{LS} value is the same as that in the preceding study of ${}^9\text{Li}$ [20]. The parameters of the central force are chosen so as to reproduce the $2n$ separation energy in ${}^9\text{Li}$ shown in Table I. In the calculation for ${}^9\text{Li}$, we also use two other parameter sets to see the effect of spin-orbit interaction on dineutron formation, as described later. Here, we should comment about the choice of $b = h = 0.0$ in the central force. Two neutrons in the spin-singlet channel are bound in accordance with these values, contradictory to experimental fact. Later, we show that our choices for parameters b and h barely change the qualitative features of dineutron correlation by comparing calculations using $b = h = 0.0$ with $b = h = 0.125$, which reproduces the n - n unbound feature.

B. Ground state energies and radii

The energies and radii of ${}^9\text{Li}$, ${}^{10}\text{Be}$, and ${}^{9,10}\text{C}$ ground states are shown in Table I. We calculate the $2n$ separation energy, S_{2n} , for ${}^9\text{Li}$ by extracting the energy of the ${}^7\text{Li}$ core as

$$S_{2n} \equiv -(\langle \Psi_M^{3/2_1^-} | H | \Psi_M^{3/2_1^-} \rangle - \langle \Psi_{\alpha+t} | H | \Psi_{\alpha+t} \rangle), \quad (14)$$

where $\Psi_M^{3/2_1^-}$ is the ground state wave function of ${}^9\text{Li}$ [Eq. (9)]. $\Psi_{\alpha+t}$ is the ground state (the first $3/2^-$ state)

of ${}^7\text{Li}$ described by the superposition of the $\alpha + t$ cluster wave functions with or without t cluster breaking. The adopted parameters in the basis wave functions for ${}^7\text{Li}$, λ_t for the degree of t cluster breaking and d_t for the α - t distance, are the same as those found in the ${}^6\text{He}+t$ cluster wave function used to describe ${}^9\text{Li}$. In a similar manner as for ${}^{10}\text{Be}$ and ${}^{9,10}\text{C}$, we evaluate the $2n$ and $2p$ separation energies, S_{2n} and S_{2p} , by extracting the $\alpha + \alpha$, $\alpha + h$, or $\alpha + \alpha$ core energy, respectively. The $2N$ separation energies for $A = 9$ nuclei, S_{2n} of ${}^9\text{Li}$ and S_{2p} of ${}^9\text{C}$, calculated with t or h cluster breaking, are reproduced as shown in Table I. For ${}^{10}\text{Be}$ and ${}^{10}\text{C}$, the two valence nucleons are slightly overbound in comparison with the experimental values. As yet, it has not proved possible to find an interaction parameter set that reproduces all the data of S_{2N} for both $A = 9$ and $A = 10$ nuclei simultaneously for the presently employed two-body effective interactions. We have determined that such overbinding is not crucial for the present results regarding $A = 10$ nuclei by adjusting the interaction parameters to reproduce S_{2N} in the $A = 10$ nuclei. The matter radii of ${}^9\text{Li}$, ${}^{10}\text{Be}$, and ${}^{10}\text{C}$ are consistent with the experimental values, except that of ${}^{10}\text{C}$ is overestimated. For calculations with core cluster breaking, the core is observed to shrink for all nuclei, which is demonstrated by the smaller values of r_p for ${}^9\text{Li}$ and ${}^{10}\text{Be}$, and by r_n for ${}^{9,10}\text{C}$, compared with those given by calculations without core cluster breaking. As a result, the mean-field potential formed by the core becomes deeper and S_{2N} becomes larger.

In the following sections, we first describe the dineutron probability in ${}^9\text{Li}$, and compare the results with and without t cluster breaking in the core to evaluate the effect of core structure changes on dineutron features. Next, we compare the dineutron features of ${}^{10}\text{Be}$ and ${}^9\text{Li}$. We also investigate the diproton correlation of ${}^{9,10}\text{C}$ and discuss the differences in the dinucleon correlation between ${}^9\text{Li}$ and ${}^9\text{C}$, and between ${}^{10}\text{Be}$ and ${}^{10}\text{C}$ in Sec. IV.

C. Effect of core structure changes on the dineutron correlation in ${}^9\text{Li}$

To investigate dineutron formation and spatial expansion from the $\alpha + t$ core in the ${}^9\text{Li}$ ground state, we examine the probability, $\mathcal{N}_{\text{dineutron}}$, for ${}^9\text{Li}$ as a function of (d_{2n}, d_t) plotted in Figs. 4(a) without t cluster breaking, and (b) with t cluster breaking. d_{2n} corresponds to the core-dineutron distance and d_t corresponds to the α - t distance. In the calculation involving t cluster breaking, the probability is enhanced in the small d_t region ($d_t \lesssim 2$ fm), indicating that the $\alpha + t$ core is shrunk. As a result of core shrinkage, the dineutron is pulled nearer the core due to the strong binding between the core and the valence neutrons, and the peak value of d_{2n} is correspondingly diminished.

We focus on the degree of dineutron formation and the spatial expansion from the core under conditions where the t cluster can or cannot be broken. To examine these

TABLE I: The total energy, the two-nucleon separation energy ($S_{2n,2p}$), and the matter, proton and neutron radii (r_m , r_p , and r_n) of the ${}^9\text{Li}$, ${}^{10}\text{Be}$, and ${}^{9,10}\text{C}$ ground states. The experimental values of the matter radii have been referred from those in Ref. [27].

		Energy (MeV)	$S_{2n,2p}$ (MeV)	r_m (fm)	r_p (fm)	r_n (fm)
${}^9\text{Li}$	w/o t breaking	-41.69	5.07	2.42	2.23	2.51
	with t breaking	-42.85	5.62	2.37	2.18	2.46
	Expt.	-45.34	6.09	2.32 ± 0.02		
${}^{10}\text{Be}$	w/o α breaking	-63.46	8.33	2.46	2.38	2.52
	with α breaking	-65.14	9.43	2.41	2.32	2.48
	Expt.	-64.98	8.38	2.30 ± 0.02		
${}^9\text{C}$	w/o h breaking	-35.86	0.76	2.45	2.55	2.24
	with h breaking	-36.73	1.04	2.42	2.52	2.21
	Expt.	-39.04	1.44	2.42 ± 0.03		
${}^{10}\text{C}$	w/o α breaking	-59.06	3.93	2.49	2.55	2.40
	with α breaking	-60.76	5.05	2.46	2.53	2.35
	Expt.	-60.32	3.73	2.27 ± 0.03		

dineutron features in more detail, we plot the dineutron probability as a function of the core-dineutron distance, d_{2n} , in Fig. 5. Here, we take the maximum amplitude of $\mathcal{N}_{\text{dineutron}}(d_{2n}, d_t)$ in Fig. 4 for each d_{2n} value. As seen in the figure, the change in the dineutron probability due to t cluster breaking is minor in the outer region of $d_{2n} \gtrsim 2.5$ fm. On the other hand, the dineutron probability in the calculation for the inner region of $d_{2n} \lesssim 2.0$

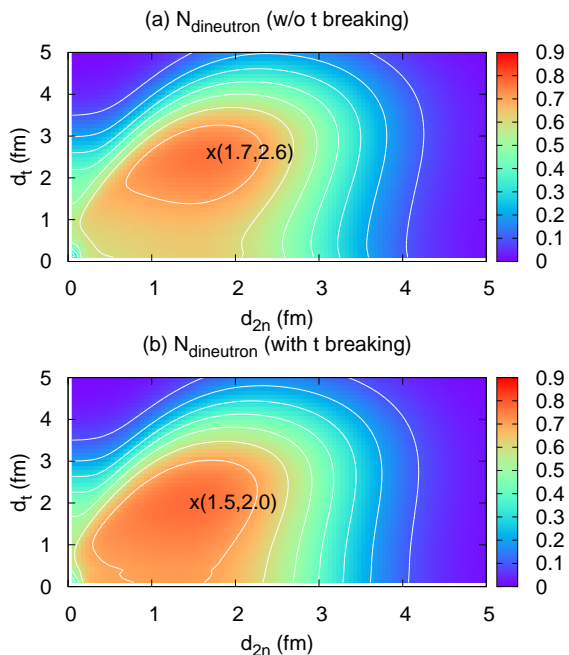


FIG. 4: (Color online) The dineutron probability, $\mathcal{N}_{\text{dineutron}}$, for the ground state of ${}^9\text{Li}$ on the d_{2n} - d_t plane. The upper figure (a) is the result without cluster t breaking, and the lower figure (b) is the result with t cluster breaking. The symbol x represents the peak position.

fm is enhanced with t cluster breaking. The key to such enhancement of the inner dineutron component is the change in the occupation probability of the $0p_{3/2}$ neutron orbits in the ${}^7\text{Li}$ core. For simplicity, we assume that the t cluster and two valence neutrons are distributed around the α cluster at a small distance. When the dineutron is distributed near the core, two neutrons in the dineutron feel the spin-orbit interaction from the core and the dineutron possibly dissociates to two independent neutrons in the major shell. Namely, the dineutron dissociation here results from competition between the dineutron (spin-singlet) component and the $(0p_{3/2})^2$ component of two neutrons around the core. In the situation where the t cluster can be broken, the two neutrons in the t cluster tend to occupy the $0p_{3/2}$ orbits to gain the spin-orbit attraction, and the $0p_{3/2}$ orbits are partially forbidden for the two valence neutrons around the ${}^7\text{Li}$ core. Consequently, the two valence neutrons cannot occupy the $0p_{3/2}$ orbits predominantly so that dineutron dissociation

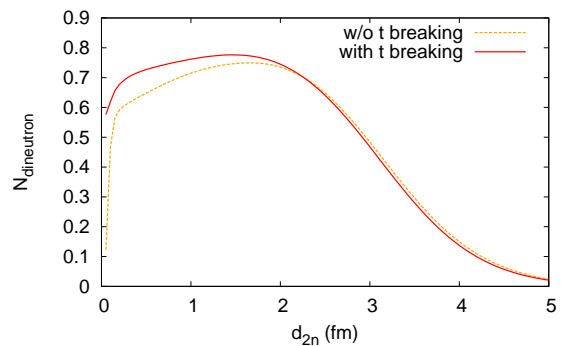


FIG. 5: (Color online) The dineutron probability, $\mathcal{N}_{\text{dineutron}}$, as a function of the dineutron-core distance, d_{2n} , in the ground state of ${}^9\text{Li}$ calculated with (solid line) and without (dashed line) t cluster breaking.

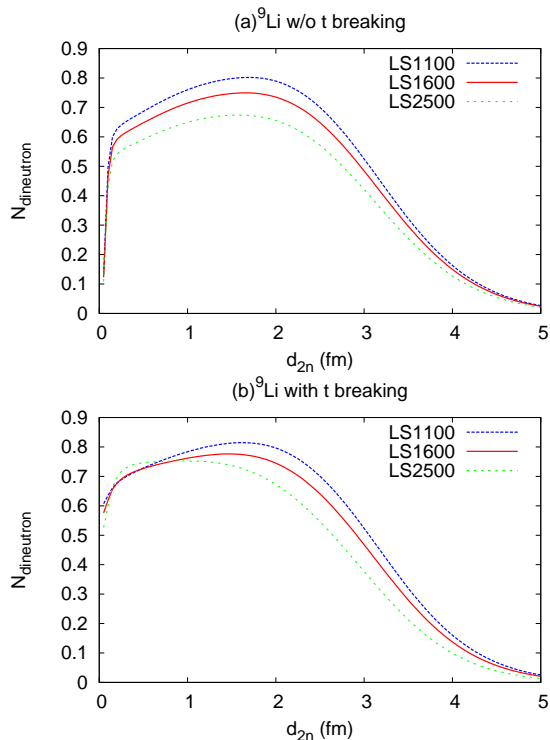


FIG. 6: (Color online) The dineutron probability, $\mathcal{N}_{\text{dineutron}}$, of the ground state of ${}^9\text{Li}$ (a) without t cluster breaking and (b) with the t cluster breaking, calculated with LS1100 (dashed line), LS1600 (solid line) and LS2500 (dotted line).

to the $(0p_{3/2})^2$ component is suppressed and the dineutron survives even in the inner region. As a result, the dineutron component is enhanced in the situation where the Pauli principle between the neutrons in the dineutron and those in the t cluster becomes significant near the α cluster (i.e., the region of small d_{2n} and d_λ shown in Fig. 4). Accordingly, we conclude that core cluster breaking, i.e., the occupation probability of the lower of the ls -splitting orbits in the core ($0p_{3/2}$ in the ${}^9\text{Li}$ case), significantly affects the degree of dineutron formation.

D. Interaction dependence of the dineutron correlation of ${}^9\text{Li}$

We show the effects of spin-orbit interaction on dineutron probability by using three interaction parameter sets having different strengths of the spin-orbit interaction, v_{LS} . The Majorana parameter, m , in the central force is adjusted to give almost the same $2n$ separation energy, S_{2n} , in the calculation with t cluster breaking. The first set has $m = 0.58$, $b = h = 0.0$, and $v_{\text{LS}} = 1600$ MeV, as used above. For the second set, where the spin-orbit interaction is weaker, we choose $m = 0.56$, $b = h = 0.0$, and $v_{\text{LS}} = 1100$ MeV. In the third, where the spin-orbit interaction is stronger, we choose $m = 0.62$, $b = h = 0.0$ and $v_{\text{LS}} = 2500$ MeV. We

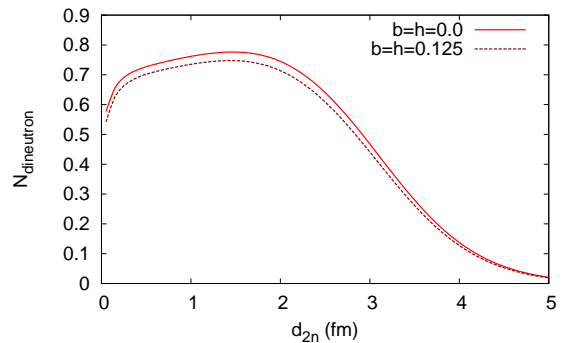


FIG. 7: (Color online) The dineutron probability, $\mathcal{N}_{\text{dineutron}}$, in the ground state of ${}^9\text{Li}$ with t cluster breaking calculated with $m = 0.58$, $v_{\text{LS}} = 1600$ MeV, and $b = h = 0$ (dashed line) and $b = h = 0.125$ (solid line).

label these parameter sets as “LS1600”, “LS1100”, and “LS2500”, respectively. The ground state energy with t cluster breaking is -43.38 MeV ($S_{2n} = 5.66$ MeV) for parameter set LS1100, -42.24 MeV ($S_{2n} = 5.87$ MeV) for LS2500, and -42.85 MeV ($S_{2n} = 5.62$ MeV) for LS1600. The dineutron probability, $\mathcal{N}_{\text{dineutron}}$, for the states with and without t cluster breaking, calculated with these parameter sets is plotted as a function of d_{2n} in Fig. 6. The dineutron probability over the entire region depends on the strength of the spin-orbit interaction in the calculations with and without t cluster breaking. These data clearly reflect that a dineutron is readily dissociated to gain the spin-orbit energy.

In the calculation with t cluster breaking, the dineutron probability inner region ($d_{2n} \lesssim 1.5$ fm) is enhanced when the spin-orbit interaction is strong. This is because, when the core cluster is largely broken due to strong spin-orbit interaction, the dineutron enhancement mechanism due to the partial blocking of the $0p_{3/2}$ orbits mentioned in Sec. III C is strongly operational.

Next, we show the dependence of the dineutron correlation on the strength of the n - n interaction. We compare the dineutron probability, $\mathcal{N}_{\text{dineutron}}$, in the ground state with t cluster breaking calculated with the original parameter set of $m = 0.58$, $b = h = 0.0$, and $v_{\text{LS}} = 1600$ MeV in addition to being calculated by adjusting the Bartlett and Heisenberg parameters in the central force to $b = h = 0.125$, which reproduces the unbounded feature of the two neutrons in the spin-singlet channel. With $b = h = 0.125$, the ground state energy of ${}^9\text{Li}$ is -40.78 MeV ($S_{2n} = 3.54$ MeV), and the two neutrons are underbound to the core, relative to the calculation with $b = h = 0.0$, because of the weaker n - n interaction. We plot their dineutron probability in Fig. 7. In the state calculated with $b = h = 0.0$, the dineutron probability is certainly larger because of the stronger n - n interaction. However, the amplitudes are not so different and the dineutron features seem to be almost the same qualitatively in these calculations.

E. Comparison the dineutron correlation of ^{10}Be with that of ^9Li

Here, we consider the dineutron probability in the ^{10}Be ground state and compare it with that of ^9Li . We also examine the effect of core structure change on the dineutron probability of ^{10}Be , and clarify the differences between dineutron features in ^{10}Be and ^9Li .

Fig. 8 shows the dineutron probability, $\mathcal{N}_{\text{dineutron}}$, as a function of the distance between the $\alpha + \alpha$ core and a compact dineutron, d_{2n} . For ^{10}Be , the change in the probability due to core cluster breaking is quite different from that of ^9Li [Fig. 5]. The inner dineutron enhancement ($d_{2n} \lesssim 1.5$ fm) is not significant because the α cluster in the $\alpha + \alpha$ core is rigid and barely broken so that the enhancement mechanism due to the core cluster breaking in ^9Li mentioned in Sec. III C is not so applicable. On the other hand, the dineutron probability in the outer region ($d_{2n} \gtrsim 2$ fm) decreases considerably. This is because the $n\text{-}\alpha$ attraction is stronger than the $n\text{-}t$ attraction, and the $\alpha + \alpha$ core shrinkage, though it is not as notable as the $\alpha + t$ core shrinkage, markedly affects dineutron expansion from the core. Moreover, the spin-orbit interaction from the α cluster is stronger and dissociates the dineutron more readily compared with the t cluster.

Finally, we compare the dineutron probability, $\mathcal{N}_{\text{dineutron}}$, between ^9Li and ^{10}Be calculated with core cluster breaking, as shown in Fig. 9. The dineutron probability of ^9Li is larger than that in ^{10}Be over the entire region. This is because the $n\text{-core}$ attraction of ^9Li is weaker than that of ^{10}Be . As a result, the dissociation effect due to the spin-orbit attraction on the dineutron is weaker, and, consequently, the dineutron can be readily formed in the inner and surface regions and distributed to the outer region from the core for ^9Li . It can be concluded that both the dineutron spatial expansion from the core and the degree of dineutron formation strongly depend on the core structure.

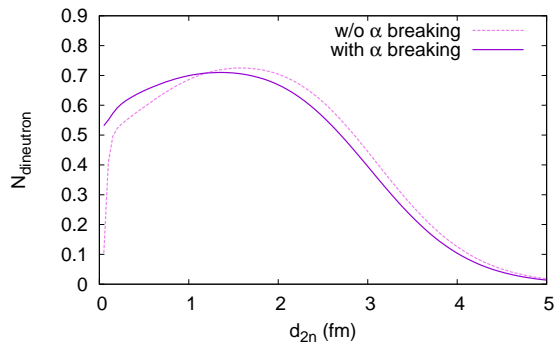


FIG. 8: (Color online) The dineutron probability, $\mathcal{N}_{\text{dineutron}}$ in the ground state of ^{10}Be calculated with (solid line) and without (dashed line) α cluster breaking.

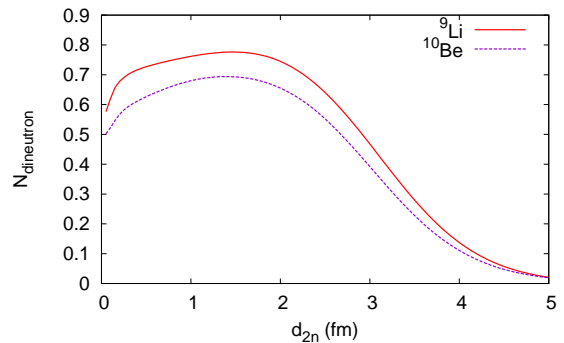


FIG. 9: (Color online) The dineutron probability, $\mathcal{N}_{\text{dineutron}}$, in the ground states of ^9Li (solid line) and ^{10}Be (dashed line) calculated with core cluster (t or α) breaking.

IV. DIPROTON CORRELATION IN $^{9,10}\text{C}$

In Sec. III we discussed the compact dineutron probability in the ground states of ^9Li and ^{10}Be . In this section, we investigate diproton correlation of $^{9,10}\text{C}$, which are the mirror nuclei of ^9Li and ^{10}Be . To begin with, we compare the diproton probability of $^{9,10}\text{C}$ and the dineutron probability of ^9Li and ^{10}Be and show that there are no qualitative differences between them. Next, we discuss the quantitative differences between dineutron and diproton correlation in more detail. We investigate the dinucleon-size changes of ^9Li and ^9C , and clarify the Coulomb effects of the dinucleon features.

A. Comparison between the dinucleon correlation of ^9Li , ^{10}Be , and $^{9,10}\text{C}$

First, we elaborate on the differences in structure and binding of the valence nucleons of ^9Li , ^{10}Be , and $^{9,10}\text{C}$, as shown in Table I. In the following section, we discuss the results with core cluster breaking. For ^9C , the two valence nucleons are bound more loosely than those for ^9Li , which is indicated by the smaller value of S_{2N} shown for ^9C ($S_{2p} \sim 1.0$ MeV for ^9C and $S_{2n} \sim 5.6$ MeV for ^9Li). Such loose binding originates in the Coulomb force, mainly between the $\alpha + h$ core and the valence protons. However, in spite of such loose core- N binding, the spatial expansion of the valence protons of ^9C is almost the same as that of the valence neutrons of ^9Li , which is seen by the proton radius of ^9C ($r_p \sim 2.52$ fm) being not significantly different from the neutron radius of ^9Li ($r_n \sim 2.46$ fm). This is because the Coulomb barrier formed by the core prevents the valence protons from spreading far from the core. Additionally, since the neutron radius of ^9C ($r_n \sim 2.21$ fm) is as large as the proton radius of ^9Li ($r_p \sim 2.18$ fm), we suppose that the $\alpha + h$ core structure of ^9C is not so different from that of the $\alpha + t$ core of ^9Li . Also for ^{10}Be and ^{10}C , the expectation values of the radii are similar to each other and there seems to be no difference in their structures.

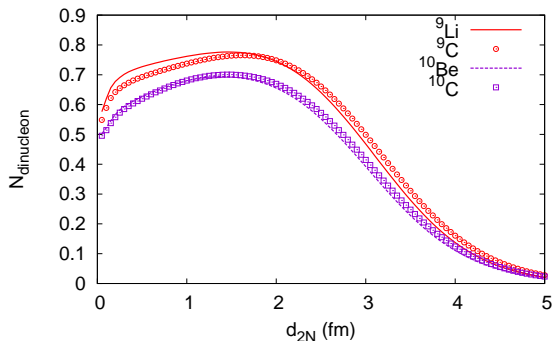


FIG. 10: (Color online) The dinucleon probability, $\mathcal{N}_{\text{dinucleon}}$, in the ground state of ${}^9\text{Li}$ (solid line), ${}^{10}\text{Be}$, (dashed line), and ${}^{9,10}\text{C}$ (open circle and square symbols, respectively) calculated with core cluster breaking.

Therefore the Coulomb force does not change the fundamental structure of these nuclei, which are not extremely loosely bound systems.

Next, we consider the diproton probability, $\mathcal{N}_{\text{diproton}}$, which is the component of a compact diproton at a distance of d_{2p} from the core, defined in the same way as the dineutron probability of Eq. (12). The dinucleon probability, $\mathcal{N}_{\text{dinucleon}}$, of ${}^9\text{Li}$, ${}^{10}\text{Be}$, and ${}^{9,10}\text{C}$ is shown in Fig. 10. Comparing these results for ${}^9\text{C}$ and ${}^9\text{Li}$, the difference in the dinucleon probability is not so remarkable in spite of a rather large difference in S_{2N} because the diproton expansion from the core is suppressed by the Coulomb barrier which the core forms. The differences between ${}^{10}\text{C}$ and ${}^{10}\text{Be}$ are smaller still. The Coulomb effect is surely minor for dinucleon correlation, but it should affect it quantitatively, more or less. In the following section, we clarify the quantitative differences between the diproton features of ${}^9\text{C}$ and the dineutron features of ${}^9\text{Li}$.

B. Quantitative differences between dineutron and diproton features

In this subsection, we discuss the Coulomb effect on dinucleon features, especially the dinucleon size. We first investigate the Coulomb effect on the dinucleon size quantitatively by comparing the diproton in ${}^9\text{C}$ with the dineutron in ${}^9\text{Li}$. Here, to consider the change in the dinucleon size, we show the overlap with the DC wave function, \mathcal{N}_{DC} , depending on the dinucleon size and expansion from the core in the ground states of ${}^9\text{Li}$ and ${}^9\text{C}$, defined in Eq. (11). The core of the test DC wave function used to measure the dineutron component is the $\alpha + t$ or $\alpha + h$ cluster wave function described in Sec. II B, which is characterized by the parameters $d_{t,h}$ (the relative distance between the α and the t or h clusters) and $\lambda_{t,h}$ (the degree of t or h cluster breaking). We fix $(\lambda_{t,h}, d_{t,h}) = (0.4, 2.0)$ so as to provide a sufficiently large overlap with the ground state of ${}^9\text{Li}$ or ${}^9\text{C}$, and this set is reasonable for the $\alpha + t$ core of ${}^9\text{Li}$ or the $\alpha + h$ core

of ${}^9\text{C}$. We calculate the overlap with $K' = +1/2$ for the test DC wave function, which is the dominant component. By allowing b_N to vary under a certain fixed value of β in the test DC wave function, we observe a change in the dinucleon size (b_N) depending on the distribution around the core (β) in the ground states of ${}^9\text{Li}$ and ${}^9\text{C}$. We plot the dinucleon probability, \mathcal{N}_{DC} , as a function of the dinucleon size, b_N , fixing the dinucleon expansion from the core, β , to 3 and 5 fm in Fig. 11. When the dinucleon is near the core ($\beta = 3$ fm), both the dinucleon probability amplitudes of ${}^9\text{Li}$ and ${}^9\text{C}$ rapidly drop off as b_N increases in a similar way. On the other hand, when the dinucleon is far from the core ($\beta = 5$ fm), the dinucleon probability amplitude of ${}^9\text{Li}$ decreases a little more rapidly than that of ${}^9\text{C}$. This indicates that the dineutron and diproton keep almost the same compact size near the core, and that the diproton can swell more readily than the dineutron far from the core.

In the following section, we discuss in detail the reasons why there is little quantitative difference for the dinucleon-size behavior near the core while differences can be evident far from the core. To do so, we investigate how large sized spin-singlet pairs of two nucleons are energetically favored under conditions of increasing spatial expansion from the core. We consider the dinucleon energy depending on the dinucleon size, b_N , and expansion, β , (where, by definition, $b_n < \beta$) in ideal ${}^9\text{Li}$

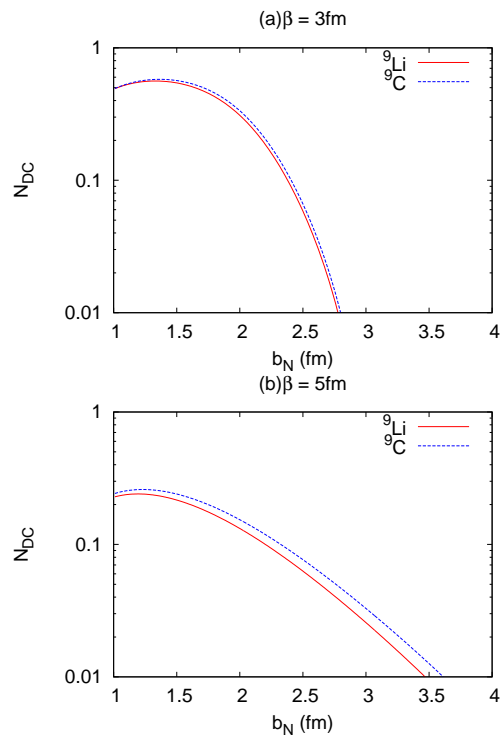


FIG. 11: (Color online) The dinucleon probability, \mathcal{N}_{DC} , of ${}^9\text{Li}$ (solid line) and ${}^9\text{C}$ (dashed line) as a function of the dinucleon size, b_N , where the dinucleon expansion from the core, β , is fixed to (a) 3 and (b) 5 fm.

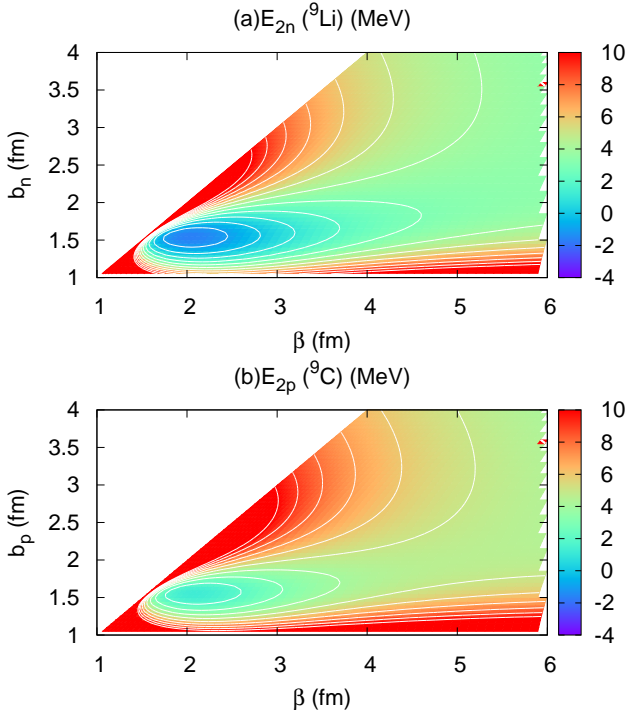


FIG. 12: (Color online) The $2N$ -energy surface of the ideal ${}^9\text{Li}$ and ${}^9\text{C}$ systems on the β - b_N plane.

($\alpha + t$ +dineutron) and ${}^9\text{C}$ ($\alpha + h$ +diproton) systems by analyzing the energy of the corresponding DC wave functions. We again evaluate the dinucleon features by changing these parameters in the DC wave function. When b_N is much smaller than β , a compact dinucleon is formed about the core. On the other hand, when $b_N \approx \beta$, each of two valence nucleons is in the single-particle s wave about the core and the dinucleon disperses because they do not have a spatial (angular) correlation. When β is small, the two valence nucleons are distributed near the core, but, when β is large, they can be expanded widely. By calculating the energy change depending on the parameters b_N and β , we see how a large dinucleon size is favored.

The aim here is to discuss quantitative changes in the dinucleon size. For this aim, the N - N interaction in the spin-singlet channel is essential. Therefore, in the following calculation, we use the values of $b = h = 0.125$ which reproduce the unbound features of a spin-singlet, two-nucleon pair, in conjunction with $m = 0.58$ and $v_{\text{LS}} = 1600$ MeV.

Here we calculate the energy of the ${}^9\text{C}$ and ${}^9\text{Li}$ DC wave functions and evaluate the $2N$ ($N = p, n$) energy with respect to the threshold energy of the core plus two free nucleons.

$$E_{2N}(\beta, b_N) = \langle \Psi_{\text{DC}}(\beta, b_N) | H | \Psi_{\text{DC}}(\beta, b_N) \rangle - \langle \Psi_{\text{DC}}^\infty | H | \Psi_{\text{DC}}^\infty \rangle, \quad (15)$$

where $|\Psi_{\text{DC}}\rangle$ is the DC wave function for ${}^9\text{Li}$ or ${}^9\text{C}$ and $|\Psi_{\text{DC}}^\infty\rangle$ is the DC wave function in the infinitely large b_n

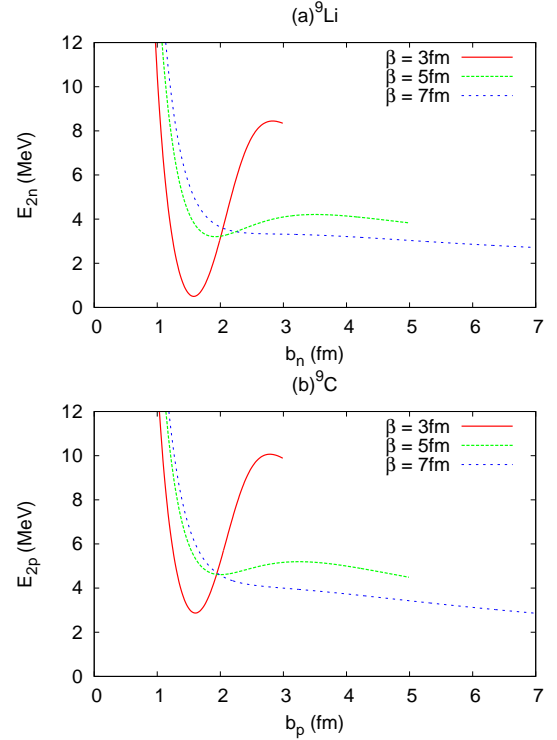


FIG. 13: (Color online) The $2N$ energy of the ideal ${}^9\text{Li}$ and ${}^9\text{C}$ systems as a function of b_N where β is fixed at 3 (solid line), 5 (dashed line), and 7 fm (dotted line).

and β limit corresponding to the system of the core plus two free nucleons. We plot the energy surfaces of the ideal ${}^9\text{Li}$ and ${}^9\text{C}$ systems on the β - b_N plane in Fig. 12. Their absolute values are quite different over the entire region due to the Coulomb interaction, but the structures of their energy surfaces show similar features wherein an energy valley exists along the $b_N \sim 1.5$ fm line (corresponding to a compact dineutron) and an energy barrier is formed in the region of $b_N \sim \beta$ (corresponding to two nucleons with little spatial correlation). Such an energy structure is the very dineutron downsizing mechanism discussed in our previous work [11]. The energy barrier is formed due to the Pauli repulsive effect from the core, and the energy valley is formed due to the attraction from the core. As a result of such an energy structure due to the core effect, a state containing a compact dinucleon is favored energetically, especially near the core. An energy barrier and valley exist for both ${}^9\text{Li}$ and ${}^9\text{C}$; therefore, a compact dinucleon can be formed for both systems. We should note that, for realistic nuclei, the dinucleon dissociation due to the spin-orbit interaction also becomes significant depending on the core structure, as shown in Sec. III, and that, actually, formation and dissociation compete with each other. However, a compact dinucleon surely can be formed by this downsizing mechanism, at least for these light-mass nuclei.

To show the dinucleon-size dependence of the $2N$ en-

ergy more clearly, we plot the $2N$ energy as a function of b_N with β fixed to a certain value, which confines the valence nucleons to a finite region whose expansion is characterized by β . We therefore plot the $2N$ energy as a function of b_N for $\beta = 3, 5$, and 7 fm, as shown in Fig. 13. It can be clearly seen both for ${}^9\text{Li}$ and ${}^9\text{C}$ that an energy pocket exists at $b_N \sim 1.5$ fm and that a high energy barrier exists at $b_N \sim \beta$ when two valence neutrons are distributed near the core ($\beta = 3$ fm). The pocket becomes shallower and the barrier becomes lower in the $\beta = 5$ case and they disappear in the $\beta = 7$ case. This is because two valence nucleons can be distributed far from the core in the larger β case so that the core effect, which is the basis of the observed energy pocket and barrier, becomes minor. The qualitative energy behavior is similar and, therefore, for ${}^9\text{C}$ as well as ${}^9\text{Li}$, a compact dinucleon can be formed near the core despite the Coulomb force acting between the two protons.

Although an energy barrier and pocket similarly form for both ${}^9\text{Li}$ and ${}^9\text{C}$, the energy difference between the barrier (the local maximum at $b_N \sim \beta$) and the pocket (the minimum at $b_N \sim 1.5 - 2$ fm) is somewhat different. The absolute values of the pocket and barrier for ${}^9\text{C}$ are naturally higher than the corresponding values for ${}^9\text{Li}$ due to the Coulomb repulsion. However, the energy difference is reduced for ${}^9\text{C}$ by less than 1 MeV compared with that for ${}^9\text{Li}$ due to the Coulomb effect. When the dinucleon is distributed near the core (small β), the absolute value of the energy difference is large so that a reduction by only a few hundred keV has little contribution. On the other hand, when the dinucleon is expanded widely from the core (large β), the energy difference itself becomes lower and even a reduction by a few hundred keV can represent a significant contribution. For instance, in the case of $\beta = 5$ fm, the energy difference between the energy barrier and the pocket is 1.0 MeV for ${}^9\text{Li}$ and the difference reduces to about a half of this value for ${}^9\text{C}$. This means that, once the valence nucleons spread to regions further from the core, the difference between the diproton and dineutron correlation—that is, the tendency for a diproton to swell and disperse more readily than a dineutron—might be seen.

${}^9\text{Li}$ and ${}^9\text{C}$ are not extremely loosely bound nuclei, in which two valence nucleons are distributed near the core. As a result, the core effect is influential to form strong dinucleon correlation, and the Coulomb effect has a minor contribution on the dinucleon correlation of the ground states of these nuclei. This is the reason why the differences between dineutron and diproton features are very small for ${}^9\text{Li}$ and ${}^9\text{C}$, and, also, for ${}^{10}\text{Be}$ and ${}^{10}\text{C}$, as discussed in Sec. IV A. However, the size change can certainly become more significant for a diproton than a dineutron at further expansion from the core. The remarkable size change in a diproton may be seen distinctively in extremely loosely bound proton-rich nuclei.

V. SUMMARY

In this work, we have investigated dinucleon (dineutron and diproton) correlation about a core in the ground states of ${}^9\text{Li}$, ${}^{10}\text{Be}$, and ${}^{9,10}\text{C}$ using the cluster wave function and the DC wave function where core cluster breaking is taken into account.

First, we have focused on ${}^9\text{Li}$ and investigated the effect of $\alpha + t$ core structure change on dineutron correlation. In the situation that the t cluster in the core can be broken, the neutrons in the core predominantly occupy the $0p_{3/2}$ orbits to gain the spin-orbit energy. The partial blocking of the $0p_{3/2}$ orbits by the core neutrons prevents the dineutron in the inner region from being dissociated into the $(0p_{3/2})^2$ configuration. As a result, two valence neutrons favor to form a compact spin-singlet dineutron inside the nuclei, and the dineutron probability in the inner region is markedly enhanced compared with the situation when the t cluster cannot be broken. We have concluded that the occupation probability of the lower of the ls -splitting orbits in the core affect the degree of dineutron formation. In addition, we have explicitly shown that the spin-orbit interaction is essential for dineutron formation and dissociation, since a dineutron is fragile and dissociates readily due to the one-body spin-orbit interaction from the core. Next, we have investigated the effect of the $\alpha + \alpha$ core structure on the dineutron correlation of ${}^{10}\text{Be}$ and compared the dineutron feature of ${}^{10}\text{Be}$ with that of ${}^9\text{Li}$. An α cluster is more rigid and harder to be broken than a t cluster. Therefore the dineutron enhancement mechanism mentioned above is ineffective for ${}^{10}\text{Be}$, and the dineutron probability does not increase for ${}^{10}\text{Be}$ as it does for ${}^9\text{Li}$. Comparing ${}^9\text{Li}$ and ${}^{10}\text{Be}$, the dineutron probability of ${}^{10}\text{Be}$ is smaller over the entire region since the interaction between the core and valence neutrons for ${}^{10}\text{Be}$ is stronger than that of ${}^9\text{Li}$ and the dineutron is more attracted and dissociated in ${}^{10}\text{Be}$.

We have also compared the diproton features of proton-rich ${}^{9,10}\text{C}$ and the dineutron features of neutron-rich ${}^9\text{Li}$ and ${}^{10}\text{Be}$. There are no qualitative differences between them and the Coulomb effect on dinucleon correlation is minor for these nuclei. We have discussed the quantitative differences between the degree of dinucleon size change for ${}^9\text{Li}$ and ${}^9\text{C}$. We have shown that a dinucleon becomes similarly compact for both ${}^9\text{Li}$ and ${}^9\text{C}$, but that the diproton can swell more readily than the dineutron due to the Coulomb effect. However, since the nuclei considered in the present work are not extremely loosely bound nuclei and the core affects the dinucleon correlation strongly, the Coulomb effect on the dinucleon, which is inferior to the core effect, is minor in these nuclei.

We have suggested that the dinucleon features, that mainly consist of the degree of formation and the spatial expansion from the core, depend on the core structure. The occupied orbits by the core nucleons especially affect dinucleon correlation significantly. In the future, we will investigate dineutron correlation in neutron-rich Be and C isotopes to clarify the effect of the occupation

probability of the lower orbits and also the effect of core deformation on dineutron correlation.

Appendix: Details of the measurement of dineutron probability

In this appendix, we explain the detailed calculation of the existence probability of a compact dineutron, $\mathcal{N}_{\text{dineutron}}$, in ${}^9\text{Li}$. In this calculation, we fix the dineutron size to a certain value, and $\mathcal{N}_{\text{dineutron}}$ is reduced to a function of the distance (d_{2n}) between the $\alpha + t$ core and the dineutron and the distance (d_t) between the α and t clusters in the core. To calculate the dineutron probability, we prepare the wave function, $\Phi_{\text{dineutron}}^{\lambda_t}$, describing the $\alpha + t$ core with the α - t distance of d_t plus a compact dineutron spherically distributed around the $\alpha + t$ core at a distance of d_{2n} , as follows.

$$\Phi_{\text{dineutron}}^{\lambda_t}(d_{2n}, d_t) = \sum_i w_i \Phi_{\alpha+t+2n}(d_{2n}, \lambda_t, d_t; \Omega_i). \quad (\text{A.1})$$

In $\Phi_{\alpha+t+2n}$, the $\alpha + t$ core structure is characterized by the parameters λ_t (the degree of t cluster breaking) and d_t (the α - t distance). The center of mass of the core is located at the origin. The Gaussian width of the nucleons in the core is $\nu = 0.235 \text{ fm}^{-2}$. We express the spherical wave functions of two valence neutrons coupled to a spin singlet with Gaussian wave packets having the fixed width, $\nu = 0.22 \text{ fm}^{-2}$ ($b = 1.5 \text{ fm}$), which are located at the same position. The position labeled as Ω_i is a point distant from the origin by d_{2n} . We choose the apexes of the octahedron ($i = 1, \dots, 6$) and the cube ($i = 7, \dots, 14$) as Ω_i . We take the angular average in the dineutron distribution around the core by summing these 14 arrangements multiplied by a factor w_i . $w_i = 1/2 \times 1/6$ ($i = 1, \dots, 6$) and $1/2 \times 1/8$ ($i = 7, \dots, 14$). By using such factors, the wave function $\Phi_{\text{dineutron}}^{\lambda_t}$ approximately describes the system of the $\alpha + t$ core plus the compact dineutron whose distribution is predominantly the S -wave around the core. We have checked that the results do not change even if we add the number of the dineutron position.

By calculating the overlap with the wave function $\Phi_{\text{dineutron}}^{\lambda_t}$, we estimate the dineutron probability that the compact dineutron is a distance d_{2n} from the core of the α and t clusters separated by a distance d_t . In the case

of ${}^9\text{Li}$ calculated without t cluster breaking, we calculate the overlap with the wave function having $\lambda_t = 0.0 \text{ fm}$ (Eq. (12) in the text).

$$\mathcal{N}_{\text{dineutron}}(d_{2n}, d_t) = |\langle \Phi_{\text{dineutron}}^{\lambda_t=0.0}(d_{2n}, d_t) | \Psi_M^{3/2_1^-} \rangle|^2. \quad (\text{A.2})$$

In the case of ${}^9\text{Li}$ calculated with t cluster breaking, we introduce t cluster breaking also in the test wave function of Eq. (A.1). For each set of (d_{2n}, d_t), we prepare a set of wave functions of $\Phi_{\text{dineutron}}^{\lambda_t(n)}$ having $\lambda_t(n) = 0.0, 0.4$, and 0.8 fm for $n = 1, 2, 3$. We orthogonalize these wave functions by a unitary matrix U as

$$\tilde{\Phi}_{\text{dineutron}}^m(d_{2n}, d_t) = \sum_n U_{mn} \Phi_{\text{dineutron}}^{\lambda_t(n)}(d_{2n}, d_t) \quad (m, n = 1, 2, 3). \quad (\text{A.3})$$

$\tilde{\Phi}_{\text{dineutron}}^m$ span the subspace characterized by λ_t s. Calculating the summation of the overlaps with the orthogonalized wave functions, $\tilde{\Phi}_{\text{dineutron}}^m$, we estimate the dineutron probability around the $\alpha + t$ core with t cluster breaking.

$$\mathcal{N}_{\text{dineutron}}(d_{2n}, d_t) = \sum_m |\langle \tilde{\Phi}_{\text{dineutron}}^m(d_{2n}, d_t) | \Psi_M^{3/2_1^-} \rangle|^2. \quad (\text{A.4})$$

We change the parameters (d_{2n}, d_t) in these overlaps [Eqs. (A.2) and (A.4)] to investigate the core-dineutron distance and the α - t distance in the core. Also, for ${}^{10}\text{Be}$ and ${}^9\text{Li}$, we perform similar calculations as was done for ${}^9\text{Li}$.

Acknowledgments

This work was supported by a Grant-in-Aid for Scientific Research from the Japan Society for the Promotion of Science (JSPS). This work was also supported by a Grant-in-Aid for the Global COE Program ‘‘The Next Generation of Physics, Spun from Universality and Emergence’’ from the Ministry of Education, Culture, Sports, Science and Technology (MEXT) of Japan. A part of the computational calculations of this work was performed using the supercomputers at YITP. The authors would like to thank Enago (www.enago.jp) for the English language review.

[1] M. Baldo, J. Cugnon, A. Lejeune, and U. Lombardo, Nucl. Phys. A **515**, 409 (1990).
 [2] M. Matsuo, Phys. Rev. C **73**, 044309 (2006).
 [3] G. F. Bertsch and H. Esbensen, Ann. Phys. (NY) **209**, 327 (1991).
 [4] M. V. Zhukov, B. V. Danilin, D. V. Fedrov, J. M. Bang, I. J. Thompson, and J. S. Vaagen, Phys. Rep. **231**, 151 (1993).

[5] K. Arai, Y. Ogawa, Y. Suzuki, and K. Varga, Prog. Theor. Phys. Suppl. **142**, 97 (2001).
 [6] P. Descouvemont, C. Daniel, and D. Baye, Phys. Rev. C **67**, 044309 (2003).
 [7] M. Matsuo, K. Mizuyama, and Y. Serizawa, Phys. Rev. C **71**, 064326 (2005).
 [8] K. Hagino and H. Sagawa, Phys. Rev. C **72**, 044321 (2005).

- [9] P. Descouvemont, E. Tursunov, and D. Baye, Nucl. Phys. A **765**, 370 (2006).
- [10] K. Hagino, H. Sagawa, J. Carbonell, and P. Schuck, Phys. Rev. Lett. **99**, 022506 (2007).
- [11] F. Kobayashi and Y. Kanada-En'yo, Prog. Theor. Phys. **126**, 457 (2011).
- [12] V. I. Goldansky, Nucl. Phys. **19**, 482 (1960).
- [13] L. V. Grigorenko, R. C. Johnson, I. G. Mukha, I. J. Thompson, and M. V. Zhukov, Phys. Rev. Lett. **85**, 22 (2000).
- [14] L. V. Grigorenko, R. C. Johnson, I. G. Mukha, I. J. Thompson, and M. V. Zhukov, Phys. Rev. C **64**, 054002 (2001).
- [15] J. Giovinazzo, B. Blank, M. Chartier, S. Czajkowski, A. Fleury, M. J. L. Jimenez, M. S. Pravikoff, J.-C. Thomas, F. de Oliveira Santos, M. Lewitowics, et al., Phys. Rev. Lett. **89**, 102501 (2002).
- [16] L. V. Grigorenko and M. V. Zhukov, Phys. Rev. C **68**, 054005 (2003).
- [17] E. Garrido, D. V. Fedrov, and A. S. Jensen, Nucl. Phys. **A733**, 85 (2004).
- [18] L. V. Grigorenko and M. V. Zhukov, Phys. Rev. C **76**, 014008 (2007).
- [19] T. Oishi, K. Hagino, and H. Sagawa, Phys. Rev. C **82**, 024315 (2010).
- [20] Y. Kanada-En'yo and T. Suhara, Phys. Rev. C **85**, 024303 (2012).
- [21] F. Kobayashi and Y. Kanada-En'yo, Phys. Rev. C **86**, 064303 (2012).
- [22] F. Kobayashi and Y. Kanada-En'yo, Phys. Rev. C **88**, 034321 (2013).
- [23] N. Itagaki, H. Masui, M. Ito, and S. Aoyama, Phys. Rev. C **71**, 064307 (2005).
- [24] D. M. Brink, *International School of Physics "Enrico Fermi", Course XXXVI* (Academic Press, New York, 1966).
- [25] A. Volkov, Nuc. Phys. **74**, 33 (1965).
- [26] R. Tamagaki, Prog. Theor. Phys. **39**, 91 (1968).
- [27] A. Ozawa, T. Suzuki, and I. Tanihata, Nucl. Phys. **A693**, 32 (2001).